Robert Radu[1]
Department of Engineering and Architecture,
University of Trieste,
Via Alfonso Valerio 10,
Trieste 34127, Italy
e-mail: rradu@units.it

Diego Micheli
Department of Engineering and Architecture,
University of Trieste,
Via Alfonso Valerio 10,
Trieste 34127, Italy
e-mail: micheli@units.it

Stefano Alessandrini
Department of Engineering and Architecture,
University of Trieste,
Via Alfonso Valerio 10,
Trieste 34127, Italy
e-mail: salessandrini@units.it

Iosto Casula
Department of Engineering and Architecture,
University of Trieste,
Via Alfonso Valerio 10,
Trieste 34127, Italy
e-mail: iosto.casula@libero.it

Bogdan Radu
Faculty of Mechanical Engineering
and Mechatronics,
University "Politehnica" of Bucharest,
Splaiul Independentei nr. 313, Sector 6,
Bucharest 060042, Romania
e-mail: bobitaradu@yahoo.com

Modeling and Performance Analysis of an Integrated System: Variable Speed Operated Internal Combustion Engine Combined Heat and Power Unit–Photovoltaic Array

The paper presents the model of a combined heat and power (CHP) unit, based on a variable speed internal combustion engine (ICE) interfaced with a photovoltaic (PV) system. This model is validated by means of experimental data obtained on an 85 kWe CHP unit fueled with natural gas and a PV system with a rated power of 17.9 kW. Starting from daily load profiles, the model is applied to investigate the primary energy saving (PES) of the integrated CHP + PV system in several operating conditions and for different sizes of PV array. The results demonstrate the dependence of the CHP performance on the operating mode and a limited convenience of the variable speed strategy. The integrated system operation leads to performance improvements, which depend on the size of the PV component.

Introduction

The European Union energy policy is focused on the reduction by 20% of the greenhouse gas emissions, associated with a 20% increase of the energy production efficiency and of the energy produced from renewables, with respect to the 1990 levels [1,2]. The achievement of these goals requires the development of a comprehensive energy policy that has to consider all the available technologies.

The use of CHP systems, due to their capability of decreasing fuel consumption by 20–30% with respect to the same size conventional plants, may represent one of the key factors in the achievement of the above mentioned targets [3]. Such systems should be also optimized with respect to cost, assuming as independent variables the thermal and the electric loads [4].

Among the different cogeneration technologies, ICEs could be considered as one of the first choices, because of their operational advantages (reliability, relatively low costs, fast transients, etc.). They cover a wide range of sizes and can be operated with different types of fuels, making them suitable for residential, institutional, commercial, and small scale industrial loads. Usually, the ICE based CHP units are operated at constant speed, allowing for direct coupling with the generator, and are optimized in a narrow range of loads. The load control is made by throttling the charge intake, which determines low efficiencies under partial load conditions. An approach to limit the efficiency decreasing with load is the adoption of a control strategy based on the speed variation [5–7] with a frequency conversion system.

Regarding the ICE based CHP systems, this approach was applied only in few prototypal or commercial systems. The experimental data presented in Refs. [5] and [6] show that, for an 120 kW CHP system fed with methane, the variable speed strategy leads to an increase of the electrical efficiency (up to 28%) only for very low loads. No major differences, with respect to the conventional strategy, were found over 75% of electrical load. In Ref. [7], the numerical results demonstrated that, for a much smaller CHP system, with an electric output of 28 kW, the variable speed operation improves the electrical efficiency with up to 47.6%.

Solar PV represents another high potential technology for reducing locally the environmental impact, since the PV systems do not generate any greenhouse gas emission during their operation. Moreover, the PV systems are ideally suited for distributed generation and can be integrated in hybrid systems based on fuel cells and gas turbines [8] or easily coupled with CHP units.

The operation of an integrated CHP + PV system may lead to energy savings, with respect to the operation of the single systems. In fact, during the high solar irradiance period the electrical load could be entirely covered by the PV generation while the CHP unit can be switched off, reducing the wasted heat. In this way, if the electrical power outputs of CHP unit and PV array are

[1]Corresponding author.

properly balanced, the two devices complement each other featuring an improvement of the overall system efficiency.

In Ref. [9], the integrated CHP + PV system is assumed to be as a type of residential distributed generation facility that could improve the market penetration of the PV technology, while in Ref. [10] the CHP integration with different types of renewable energy systems, including photovoltaics, is seen as a way to limit the operation of the CHP unit in part load conditions, that are usually characterized by lower values of efficiency than in the nominal one.

Generally, the experimental and numerical data regarding the convenience of a variable speed ICE based CHP system are limited. Moreover, no references were founded regarding the performance of integrated system CHP + PV, when the CHP unit is operated with variable speed. Therefore, the present paper targets to investigate the above mentioned issues, by assessing the benefits that may result from the implementation of the CHP unit variable speed strategy and from the integrated operation with a PV system.

The paper presents the model of a CHP unit, based on a variable speed ICE interfaced with a PV system. This model, developed in MATLAB-Simulink, was validated by means of experimental data acquired in electrical priority operating mode on a CHP unit with 85 kW of electric power output, fueled with natural gas, and a PV system with a rated power of 17.9 kW. Starting from daily load profiles, the model was applied to investigate the PES of the integrated CHP + PV system in several operating conditions and for different sizes of PV array.

System Modeling

The simulation model is implemented in MATLAB-Simulink and consists, as shown in Fig. 1, of three main subsystems: the CHP unit, the PV system, and the load. Based on the main input, represented by the thermal and/or electrical load profile, the model calculates the operating parameters of the integrated CHP + PV system. The model main outputs are the CHP and PV operating efficiencies, presented also in terms of PESs.

CHP Unit Model. The CHP unit model was realized following the guidelines presented in Ref. [11], by means of three main blocks, each of them dedicated to a certain CHP component: the ICE and the two heat exchangers that recover heat from the exhaust gas and the cooling water.

The main inputs required by the ICE simulation block are the choice between the electrical or thermal priority operating mode of the CHP and the corresponding load profile. At every load condition, the block calculates the exhaust gas and engine coolant temperatures and the fuel consumption, i.e., the operating point. The fuel consumption is controlled by means of a proportional-integral-derivative (PID) that uses as feedback the required electrical or thermal power.

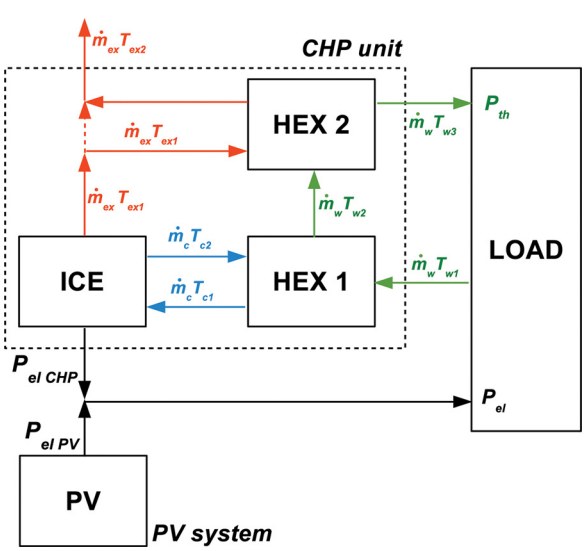

Fig. 1 Simulation model layout

The calculations are based on two operating curves, describing the variation of the mechanical power and exhaust gas temperature with the fuel power input, according to a defined load–engine speed control strategy. These operating curves can be obtained directly from experimental data or from numerical simulations regarding a specific engine. In this paper, the curves were calculated using a dedicated ICE simulation model realized with the AVL BOOST software. The runs cover a wide range of loads and speeds and take into account also the pressure loss in the exhaust gas heat exchanger. The simulation model calculates the maps of engine efficiency and exhaust gas temperatures as a function of speed and break mean effective pressure. The maps were interpolated in order to obtain the above mentioned operating curves according to two different control strategies. The first is a conventional strategy that assumes the engine operation at a constant speed of 1500 rpm, which allows the direct coupling with a 50 Hz generator. The second strategy assumes the engine operation at variable speed with load, according to a correlation obtained on the basis of available experimental data and then reproduced on the simulated performance maps, as it will be presented later in this work.

The mechanical power, P_m, and the exhaust gas temperature are thus obtained at every load condition, to which corresponds the fuel consumption value given by the control strategy of the engine.

The exhaust gas mass flow rate $\dot{m}_{ex}$ is calculated as a function of the fuel power input P_f, the air to fuel ratio (AFR), and the fuel lower heat value (LHV)

$$\dot{m}_{ex} = \frac{P_f}{LHV}(1 + AFR) \tag{1}$$

The available exhaust thermal power P_{thex} is the product of $\dot{m}_{ex}$ and the difference between the flue gas enthalpies at the exhaust and ambient temperatures.

The available engine coolant thermal power P_{thc} is obtained with Eq. (2) on the basis of the engine energy balance [11], by subtracting from the fuel power input the mechanical and the available exhaust thermal powers and the heat flux lost through the external surface of the engine. The latter is assumed equal to a given fraction x_{hl} of the fuel power input.

$$P_{thc} = P_f - P_m - P_{thex} - x_{hl} \cdot P_f \tag{2}$$

Temperatures at the engine and user sides of the cooling water heat exchanger are calculated resolving Eqs. (3)–(5), where T_{c1} and T_{c2} represent the engine coolant inlet and outlet temperature, $\dot{m}_c$ and c_{pc} are the coolant flow rate and heat capacity, ε_{HEX1} is the effectiveness of the heat exchanger, T_{w1} is the water inlet temperature, T_{w2} is the water outlet temperature (toward the exhaust gas heat exchanger), $\dot{m}_w$ and c_{pw} are the water mass flow rate and heat capacity.

$$T_{c2} = T_{c1} + \frac{P_{thc}}{\dot{m}_c \cdot c_{pc}} \tag{3}$$

$$T_{c1} = T_{c2} - \varepsilon_{HEX1}(T_{c2} - T_{w1}) \tag{4}$$

$$T_{w2} = T_{w1} + \frac{P^*_{thc}}{\dot{m}_w \cdot c_{pw}} \tag{5}$$

In Eq. (5), the recovered heat P^*_{thc} is equal to the available engine coolant thermal power, P_{thc}, if the emergency radiator is switched off, as in the case of Fig. 1.

The coolant flow rate is calculated using a lookup table that contains the cooling pump operating curve. The water mass flow rate is a characteristic of the user circuit; if the water inlet temperature is chosen as a design parameter, $\dot{m}_w$ must ensure that the outlet temperature, after the exhaust gas heat exchanger, is lower than the maximum allowable value of the user circuit. The equation system is resolved in the cooling water heat exchanger simulation block (HEX1 in Fig. 1). The simulation block of the exhaust gas heat exchanger (HEX2 in Fig. 1) calculates the recovered heat and the outlet temperatures, of both the exhaust gas and the user water, using the same simulation approach of the engine coolant heat exchanger

$$T_{ex2} = T_{ex1} - \varepsilon_{HEX2}(T_{ex1} - T_{w2}) \tag{6}$$

$$P^*_{thex} = \dot{m}_{ex} c_{pex} (T_{ex1} - T_{ex2}) \tag{7}$$

$$T_{w3} = T_{w2} + \frac{P^*_{thex}}{\dot{m}_{ex} c_{pex}} \tag{8}$$

where T_{ex1} is the exhaust gas temperature at the heat exchanger inlet, which is equal to the temperature at the engine outlet, T_{ex2} is the exhaust gas temperature after the heat recovering, ε_{HEX2} is the effectiveness of the exhaust gas heat exchanger, T_{w3} is the water outlet temperature, P^*_{thex} is the recovered heat from the exhaust gas, and c_{pex} is the flue gas heat capacity. The effectiveness of the two heat exchangers can be derived from well-known theoretical considerations based on the ε–number of transfer units method, and eventually verified experimentally.

PV System Model. The PV system simulation block works with the following inputs:

- the global solar irradiance
- the ambient temperature
- the module main characteristics (operating curves, nominal cell operating temperature, and geometry)
- the PV array characteristics (number of modules and inverter operating curves)

Regarding the solar irradiance data input, the model can operate either with the data measured on the PV array plane, for example on a south oriented panel with a 30 deg inclination angle, or with the data measured on an horizontal plane. In the last case, the irradiation data for the tilted surface are calculated as a function of the tilt angle and global horizontal solar irradiance using the Hay–Davies model [12,13].

Using the previously mentioned inputs, the model calculates the PV panel theoretical output P^t_p assuming the operation of the inverter with the maximum power point tracking strategy.

The panel electrical output P_p is calculated as the difference between the theoretical output P^t_p and the sum of temperature P_{temp}, reflection P_{ref} and system P_{sys} losses

$$P_p = P^t_p - (P_{temp} + P_{ref} + P_{sys}) \tag{9}$$

The temperature loss is calculated by means of the temperature coefficient of the panel, γ, which is the fraction of the peak power at standard test conditions, P^{STC}_p, lost for an increase of panel temperature of 1 °C with respect to the reference value $t_{STC} = 25$ °C

$$P_{temp} = (t_{STC} - t_p) \cdot \gamma \cdot P^{STC}_p \tag{10}$$

The temperature coefficient is specified by the panel manufacturer or can be experimentally detected [14].

The reflection and system losses are expressed as fractions of the theoretical output and depend on the array orientation and structure: usual values are lesser than 0.05 [15].

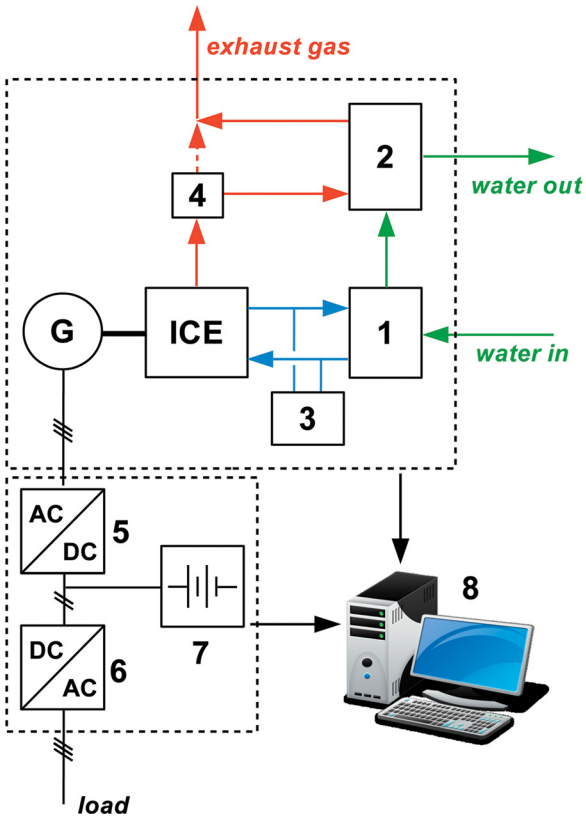

Fig. 2 CHP unit schematic: 1—engine coolant heat exchanger, 2—exhaust gas heat exchanger, 3—emergency radiator, 4—diverter valve, 5—rectifier, 6—inverter, 7—battery pack, and 8—data acquisition PC

Model Validation

The model was validated with reference to a demonstrative CHP + PV integrated system, installed in the campus of Area Science Park of Trieste (Italy). The facility is composed of a CHP unit which is able to provide a continuous electrical power output of 85 kW, interfaced with a PV array with a peak rated power of 17.9 kW.

Experimental Test Facility. The CHP unit (Fig. 2) is based on a natural gas fueled ICE coupled to an asynchronous generator. The grid connection is realized through a power electronics unit composed of a rectifier followed by the inverter. With this configuration, the CHP unit delivers a constant output frequency of 50 Hz, while the engine operates with a variable speed strategy that may lead to improvements of the ICE operating efficiency, especially under part load conditions.

The thermal power recovery system has the typical layout composed of an engine coolant/water heat exchanger and an exhaust/water heat exchanger. In case of low demand, the thermal power can be dissipated on an emergency radiator.

The CHP and ICE main characteristics are summarized in Tables 1 and 2, respectively.

The PV array contains 78 Sanyo HIP-230 HDE1 panels, each one with a rated power of 230 W (Fig. 3) and an efficiency of 16.6% [16]. The main characteristics of the PV array are presented in Table 3. The inverters, as shown in Fig. 4, operate with a maximum efficiency around 97.8%.

As Fig. 5 presents, each inverter was monitored using a multifunction device (MFD) that measures and stores the AC electrical parameters. The MFD acquires, using current and voltage dedicated modules, the DC electrical parameters for each string that is

Table 1 CHP main characteristics

Engine type	SI, 4 stroke, nat.aspirated
Fuel	Natural gas
Generator	Asynchronous, air cooled
Operation	Variable speed
Power electronics	Rectifier/AC converter
Storage/UPS	Pb batteries
Continuous electric power	85 kW
Peak electric power	130 kW (for 15′)
Output frequency	50 Hz
Maximum electrical efficiency	31%
Thermal power	170 kW
Maximum thermal efficiency	60%

Table 2 ICE main characteristics

Engine type	GM Vortec 8100
Cylinder arrangement	8V
Total displacement	8128 cc
Bore × stroke	107.95 × 111 mm
Compression ratio	9.1:1
Fuel	Natural gas
Fuel system	Electronically contr. carburetor
Air/fuel ratio	Stoichiometric
Maximum power	171 kW at 2800 rpm
Maximum torque	632 Nm at 1800 rpm
Emission control system	TWC

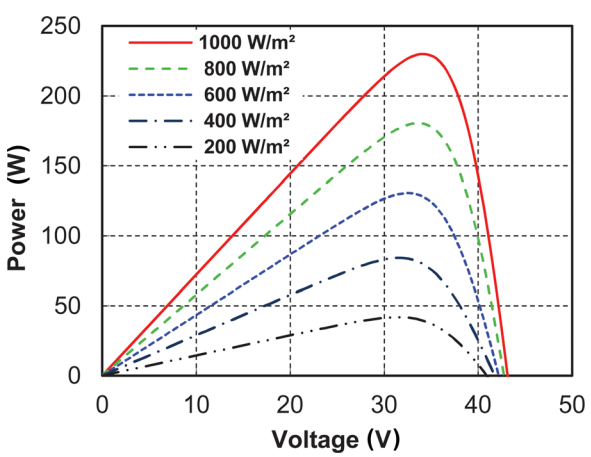

Fig. 3 PV panel power curves

Table 3 PV array main characteristics

Rated power (kW)	17.9	
Module manufacturer	Sanyo	
Module type	HIP 230 HDE1	
Module efficiency[a] (%)	16.6	
Module rated power[a] (W)	230	
Number of modules	78	
Module tilt (deg)	30	
Module orientation (deg)	180	
Number of inverters	2	
Inverter manufacturer	Aurora	
Inverter number	#1	#2
Inverter type	PVI-10	PVI-10
Strings/inverter	3	3
Modules/string	13	13

[a]Standard test conditions: air mass 1.5, irradiance = 1000 W/m^2, and cell temperature = 25 °C.

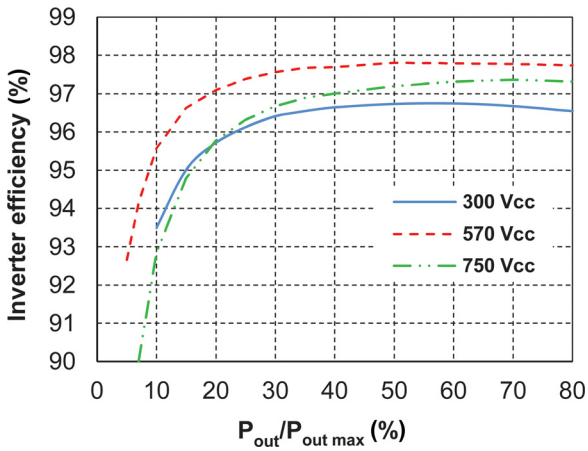

Fig. 4 Inverter operating curves

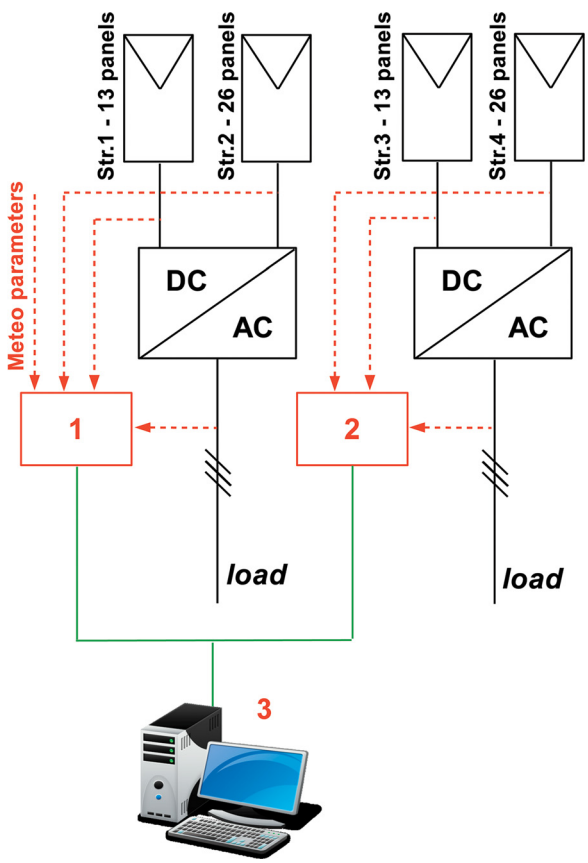

Fig. 5 PV system diagram: 1 and 2—multi function device and 3—remote monitoring PC

connected to the inverter. Both DC and AC electrical parameters were acquired with a maximum error of 0.5%. The MFD also receives and stores the data from other sensors; in particular it stores the solar irradiance and both panel and ambient temperatures.

The solar irradiance was measured with two secondary standard Kipp & Zonen CMP 11 pyranometers. The first has the same positioning (tilt and orientation) as the PV panels, while the second measures the irradiance in the horizontal plane.

As presented in Fig. 6, the electrical power produced by both ICE based CHP unit and PV array may be directed, by means of a control cabinet (CCAB), to the electricity grid or to a load bank. As far as the CHP unit is regarded, the thermal power may be

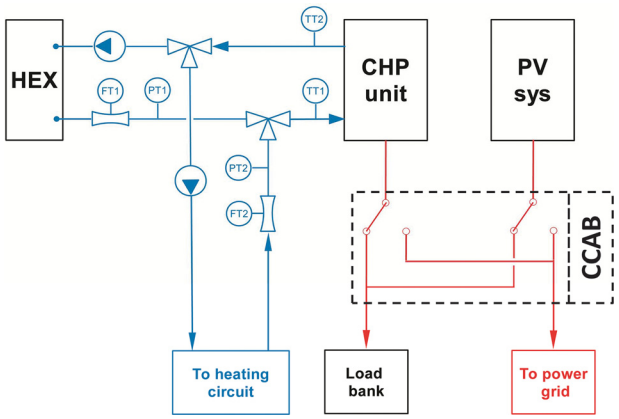

Fig. 6 Integrated system schematics

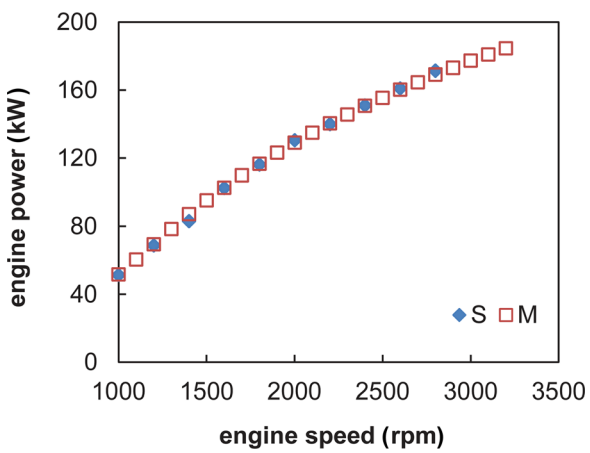

Fig. 7 Comparison between ICE simulated (S) and manufacturer (M) data of engine power—full load

delivered to the heating circuit or to the thermal load bank (HEX) which is aimed to dissipate the heat developed by the CHP unit.

By coupling the integrated CHP unit and the PV array to the electric and thermal load banks, the system can be completely set in island mode. The electric load bank used in the preliminary tests is of the resistive type and allows load variation with a minimum step of 5 kW. The thermal load bank allows a continuous variation of the amount of dissipated heat, based on the user set point.

Model Validation Procedure. The validation procedure regarded the three main subsystems of the simulation model: the ICE alone, the whole CHP unit, and the PV array.

As far as the ICE is concerned, the AVL Boost simulation model considers the engine V8 configuration with identical cylinders, fuelled with natural gas. The engine modeling is based on standard components available in the software libraries, i.e., pipes and junctions, cylinders, fuel injectors, exhaust mufflers, and catalytic converters. Several mathematical models integrated in the AVL Boost platform were used. The combustion was considered stoichiometric and was simulated with the fractal model, very sensible at load and speed changes. This model divides the combustion chamber in two zones containing the burned gas and the fresh mixture. The main reason for the choice of the fractal model is that, once the model parameters are adjusted for a given fuel and operational conditions, it is not necessary to readjust the parameters when a different fuel is used. In our case, this could be useful for the assessment of the engine operation with different types of

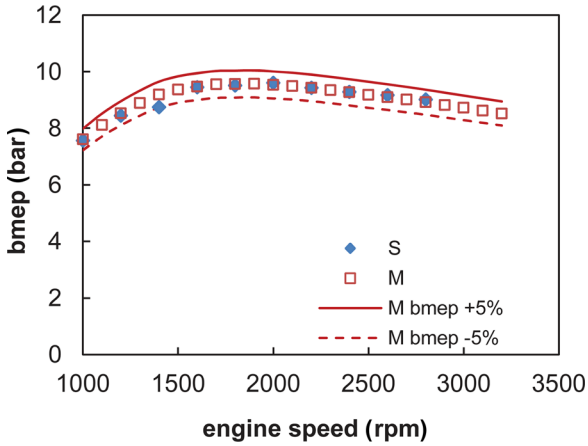

Fig. 8 Comparison between simulated (S) and manufacturer (M) data of brake mean effective pressure—full load

gaseous fuels. For the heat transfer calculation, the Woschni model was chosen, while the friction losses were modeled with the Patton, Nitschke, and Heywood model as presented in Refs. [17] and [18]. The simulation results were compared with the engine manufacturer data regarding power and brake mean effective pressure for the full load conditions and natural gas fuelling [19]. The comparison, presented in Figs. 7 and 8, demonstrates a good agreement between numerical and manufacturer data. The maximum difference between the two sets of data (4.8%) was founded for the break mean effective at the engine speed of 1500 rpm.

In partial load conditions, the comparison was realized, in terms of engine efficiency, between the numerical results and the experimental data acquired on the CHP unit operated with the variable speed strategy. The mechanical power, used for the engine efficiency calculation, was determined from the ratio between the measured electrical power and the efficiency of the electrical generator, provided by the manufacturer specifications and equal to 0.95. Figure 9 presents the variable speed engine operating curve measured with the CHP in electric priority, at different part load conditions, superimposed on the efficiency map, calculated by means of the AVL Boost simulation. For each analyzed operating point, the figure shows the difference between the calculated and experimental engine efficiencies, represented as circles with radius proportional to the error value. As one can see, the numerical simulation approximates in a good manner the experimental data, with a maximum difference of 5.26% for the lowest investigated load. The positioning of the variable speed engine operating curve on the calculated efficiency map confirms that this strategy allows to maintain, especially for low power outputs, the engine operating point in efficiency zones higher than in the case of constant speed operation at 1500 rpm.

The overall model of the CHP unit was validated through comparison between numerical and experimental or manufacturer values of electrical and thermal efficiencies, obtained in various steady state conditions. At each condition, the engine rotational speed is defined by the variable speed strategy as shown in Fig. 9. As far as the electric efficiency is concerned, the data are presented in Fig. 10. The numerical results underestimate the manufacturer values, up to a maximum difference of −6.5%, which is comparable with the maximum −5% error on bmep observed in Fig. 8 at 1400 rpm (but it must be taken into account that the load conditions in the two figures are different). The results appear to get better if the experimental data are considered: in this case the model slightly overestimates the efficiency values, with a maximum difference of +3%. As a whole, the CHP simulation model demonstrates a sufficiently good precision with respect to the electric efficiency. Regarding the thermal efficiency, Fig. 11 shows

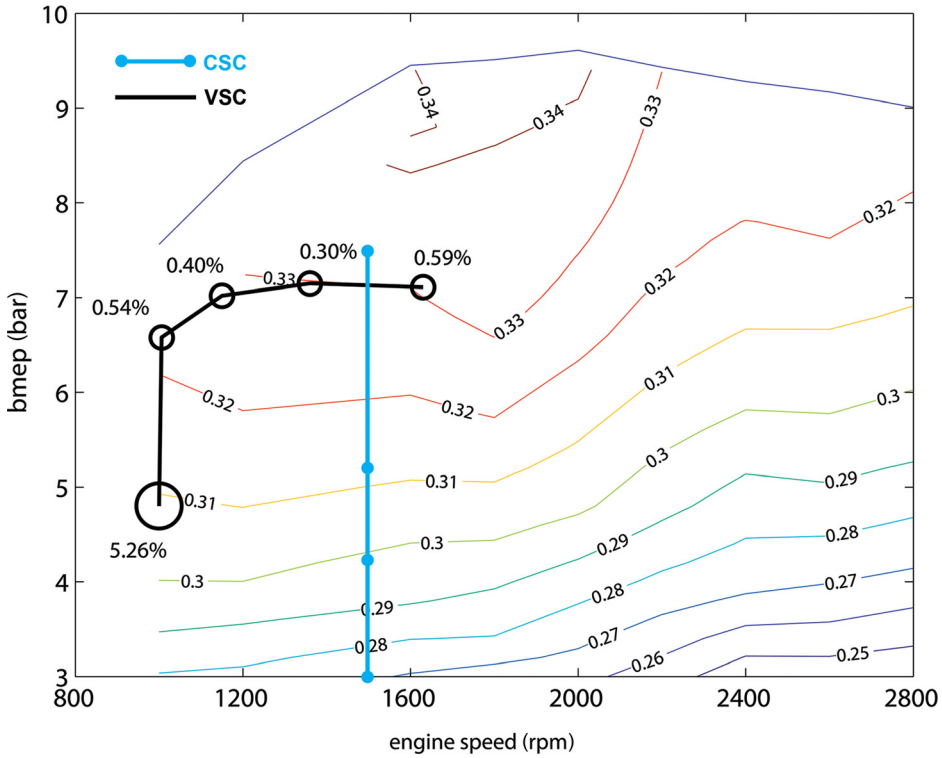

Fig. 9 Simulated efficiency map. Variable speed strategy operating curve (VSC—experimental) versus constant speed strategy operating curve (CSC—simulated).

the comparison only between the manufacturer and simulated data. During the experimental phase, a malfunctioning of the emergency radiator determined an excessive waste of heat, which had no effect on the engine operation but gave low values of the thermal efficiency, which were considered as not reliable. It should be noticed that the simulation model underestimates the thermal efficiency up to −10%: remembering also the above error on the electric efficiency, this will require further experimental investigation, to verify the effectiveness of the manufacturer data in the operating conditions of the facility.

As an example, Table 4 shows the values of the main operating parameters and simulation results obtained for an electrical load of 78 kW, with the variable speed control strategy.

The PV system simulation was validated by comparing the calculated and measured power outputs, both in DC and AC. Figure 12 presents, as an example, the comparison between the simulated and measured DC power curves for a day (Oct. 18, 2011) with a maximum global irradiance of 480 W/m^2, measured on a horizontal plane. Two simulated power curves are considered: the S1 was calculated with the global irradiance data measured on the tilted PV panel plane, while S2 was determined using the irradiance data measured on the horizontal plane.

The S1 curve approximates with a good accuracy the experimental data with a maximum difference, considering the higher irradiance hours, of about 2.8%. The same difference for the S2 simulated curve increases up to 8%. This lower simulation

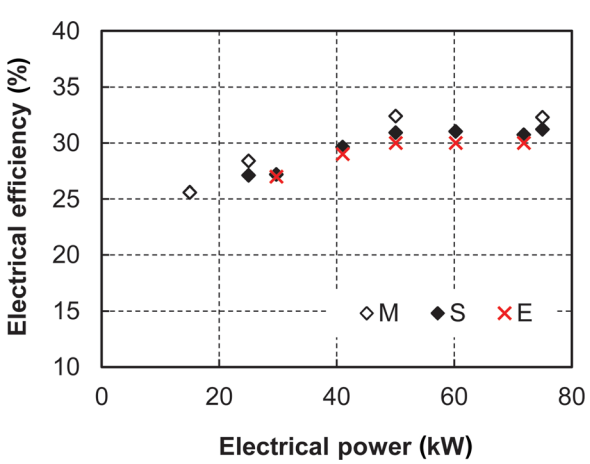

Fig. 10 Electrical efficiency variation with the electrical power: M = manufacturer data, S = simulation data, E = experimental data. Variable speed strategy.

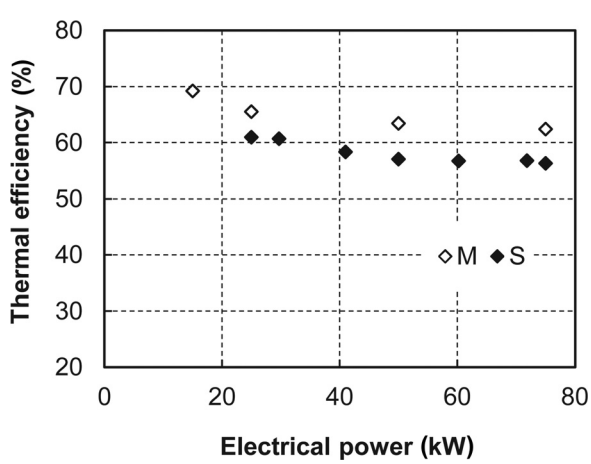

Fig. 11 Thermal efficiency variation with the electrical power: M = manufacturer data, S = simulation data. Variable speed strategy.

Table 4 Example of CHP model main parameters and simulation results

ICE	
Speed (rpm)	1688
Fuel	Natural gas
Power (kW)	78.21
Bmep (bar)	6.84
Coolant flow rate (kg/s)	2.885
Fuel consumption (kg/s)	0.0049537
Air consumption (kg/s)	0.0852
ICE efficiency	0.329
Engine coolant inlet temperature T_{c1} (°C)	73.6
Engine coolant outlet temperature T_{c2} (°C)	79.9
CHP unit	
Heating water flow rate mW (kg/s)	2.3
Inlet temperature T_{w1} (°C)	70
Intermediate temperature T_{w2} (°C)	77.8
Outlet temperature T_{w3} (°C)	84.2
Exhaust gas temperature (°C)	753.3
Exhaust gas outlet temperature (°C)	179.1
Electrical output (kW)	74.3
Thermal output (kW)	137
Electrical efficiency	0.312
Thermal efficiency	0.576
HEX1 effectiveness	0.630
HEX2 effectiveness	0.850
Dissipated heat (5% of the fuel input) (kW)	11.89

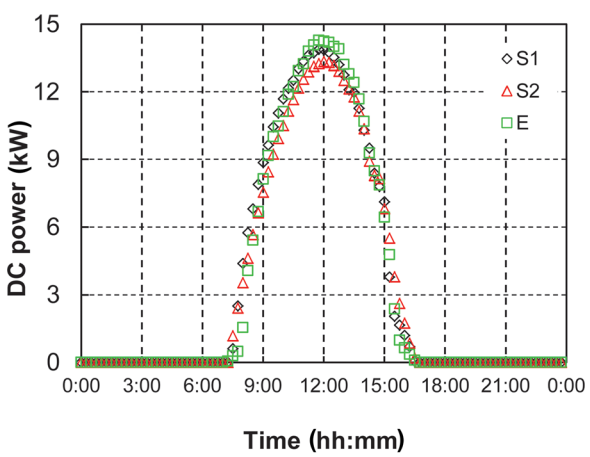

Fig. 12 Comparison between the simulated power output curves (S1 and S2) and the measured data (E) for the PV array

accuracy could be related to the errors induced by the Hay–Davies model when calculating the solar irradiance on the tilted plane.

CHP and Integrated CHP + PV Systems Performance Analysis Results

The validated model was used to carry out several simulations, in different configurations, in order to assess the benefits that may result from the CHP unit operation with variable speed strategy and from the operation of the integrated CHP + PV system. Performance are analyzed in terms of values of the PES index that has been calculated according to the European Directive No. 2004/8/CE and the related Italian decree D.M. 05/2009/11.

The PES is defined as

$$\mathrm{PES} = \left(1 - \frac{1}{\frac{\eta_{\mathrm{th,CHP}}}{\eta_{\mathrm{th,ref}}} + \frac{\eta_{\mathrm{el,CHP}}}{\eta_{\mathrm{el,ref}}}}\right) \cdot 100 \qquad (11)$$

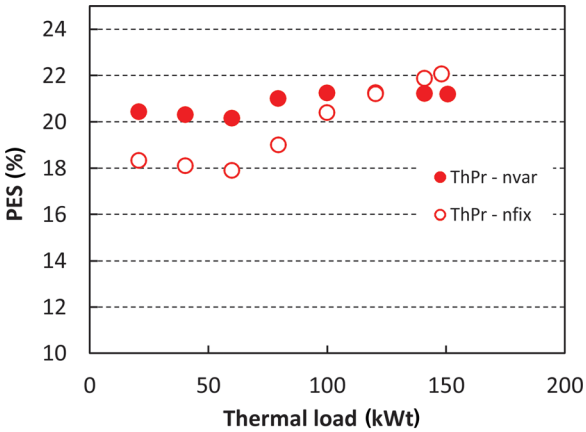

Fig. 13 PES index in thermal priority mode for constant (nfix) and variable speed (nvar) strategies, CHP unit only

Where $\eta_{\mathrm{th,CHP}}$ and $\eta_{\mathrm{el,CHP}}$ are the thermal and electrical efficiencies of the CHP unit. The reference thermal efficiency is $\eta_{\mathrm{th,ref}} = 90\%$, while the reference electrical efficiency is $\eta_{\mathrm{el,ref}} = 49\%$.

System Performance Baseline. The first results, obtained in thermal priority mode at various thermal loads, considering only the CHP unit and assuming the complete utilization of the cogenerated thermal power, are presented in Fig. 13. Due to the last hypothesis, the reported PES values must be considered as the maximum that could be obtained in real operating conditions, with reference to perfectly optimized CHP applications. The curves demonstrate that the variable speed strategy offers a real operating advantage only for part loads, while for the full load operation the constant speed strategy determines a slightly better performance.

Anyhow, with both strategies the considered CHP plant can be classified as a high efficiency one, since the PES values are always higher than the lower legal limit (0% for small plant with electric power less than 1 MW, 10% for larger units). The results are similar to those presented in Ref. [5] and are strictly related to the operating curves presented in Fig. 9 in the "Model Validation" section. Theoretically, for the high loads, slight improvements may be obtained by adopting an operation curve closer to the maximum torque, allowing higher efficiencies. Nevertheless, in this case, the influence of the increased mechanical stresses on engine durability must be evaluated.

System Performance With Variable Load Profiles. As mentioned, the PES values previously presented, with different thermal load levels, should be considered as a maximum baseline. If the CHP unit operates in thermal priority, following a certain load profile, the expected PES values will be placed between the minimum and maximum values presented in Fig. 13. If the CHP unit operates in electrical priority mode, eventually with partial heat recovery, lower PES values must be expected.

To evaluate the system performance under variable load conditions, in thermal and electrical priority operating modes, two simulation cases were considered:

Case No. 1: Thermal priority with an imposed load profile, without the integrated PV system;

Case No. 2: Mixed thermal–electrical priority operating mode, with and without the integrated PV system. In this case, the influence of the PV size was also evaluated.

Typical residential thermal and load profiles were considered. Lighting, home appliances, and air conditioning systems were considered for the electrical load, while heating and hot water were included in the thermal one. The thermal and electrical load profiles were imposed as suggested in Ref. [20] as normalized

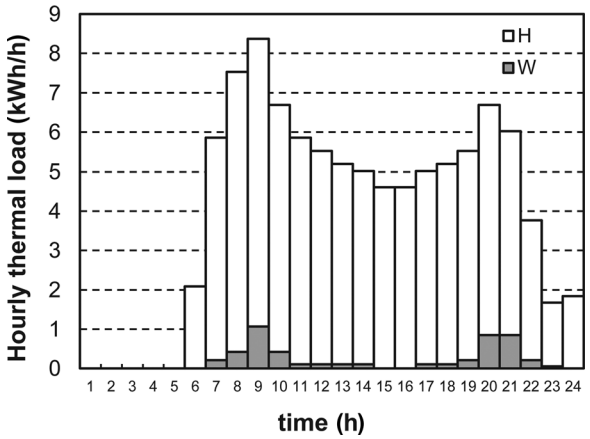

Fig. 14 Hourly thermal load for one apartment, month of January (H = heating, W = hot water)

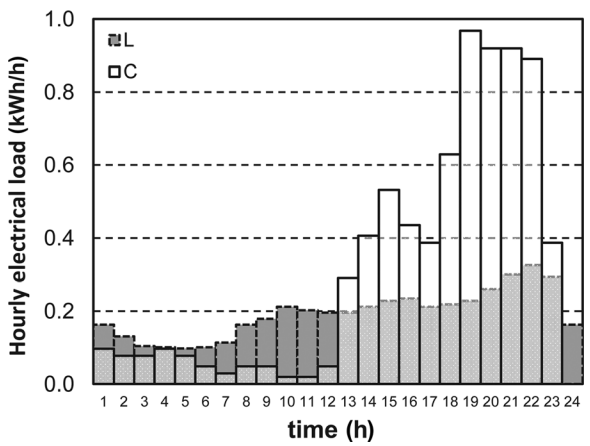

Fig. 15 Hourly electrical load for one apartment, month of July (L = lighting, C = air conditioning)

Table 5 Variable load simulation results. Thermal priority, CHP only.

	PES (%)	
	Thermal priority, CHP only	
Apartments	Constant speed	Variable speed
100	21.32	21.10
50	21.23	21.08
30	20.75	21.04

average daily profiles, specific for each month, for a residential building with an imposed number of 100 m^2 apartments. The maximum thermal load for a single apartment was set equal to 9.5 kWh/h (8.4 kWh/h for heating plus 1.1 kWh/h for hot water, in January at 9 am) according to the EPBD Italy's Country Report [21]. The maximum electrical load was set equal to 1.2 kWh/h (0.9 kWh/h for air conditioning plus 0.3 kWh/h for lightning, in July at 9 pm) according to the final report of the MICENE [22] project, which regards the electrical power consumptions in the Italian household sector. The thermal and electrical load profiles for the above mentioned months, for a single apartment, are presented in Figs. 14 and 15.

During the simulated period of 365 days, the variability of the thermal load can be attributed to the heating requirement that varies with the ambient temperature, while the hot water component has the same profile for the entire year [20]. The electrical load variation is related to the air conditioning system consumption, which occurs in the summer months. The daily lighting load profile was kept constant, for the entire year [20].

The simulation considers a minimum number of 30 apartments for which, in thermal priority mode, the CHP unit is able to cover almost the entire thermal request (96%), but operating only 9% of the time at full load. For the maximum number of 100 apartments, the CHP unit covers only 78% of the thermal request, operating at full load 30% of the time. A further increase of the full load operation time to about 50% is possible with a number of 200 apartments. This was not considered in our simulations, since the thermal load coverage by the CHP unit resulted very low. The remaining thermal load should be covered with an additional boiler.

In order to evaluate the PV system output, the model uses the daily solar irradiance curves during the entire simulated period of 365 days, calculated with the online PVGIS software [23], assuming clear sky conditions. This and the constant lighting load profile are simplifying hypothesis, adopted for all simulation cases, which should not affect the significance of our comparative analysis.

The results of the simulation case no. 1, presented in Table 5, demonstrate that by applying the variable speed strategy, the PES index remains practically unchanged with the load. The variable speed operation has a very limited convenience only for the lowest number of apartments, a result that is coherent with the data presented in Fig. 13. Only for the lowest thermal loads, the variable speed strategy allows for slightly higher efficiencies of the ICE, with respect to the constant speed strategy, which leads to limited improvements of the PES index.

The operation in thermal priority mode during summer time has a relatively limited significance from a practical point of view, since the CHP unit must cover very low loads. A more advantageous alternative might be the operation of the CHP during summer in electrical priority mode, eventually with the integration of a PV system.

Simulation case no. 2 considers such a mixed operating mode, with the operation in electrical priority from April to September and thermal priority in the rest of the year. The PV array rated power was initially set to 17.9 kW, equal to the output delivered by the experimental system. In order to analyze the influence of

Table 6 Variable load simulation results. Mixed operating mode.

	PES (%)			
	Mixed operating mode, CHP only		Mixed operating mode, CHP + PV(17.9 kW)	
Apartments	Constant speed	Variable speed	Constant speed	Variable speed
100	4.62	5.69	6.23	7.06
50	8.39	10.04	10.50	11.70
30	9.57	11.96	12.13	13.94

Table 7 Variable load simulation results. Influence of the PV array output on the integrated system performance.

	PES (%)		
	Mixed operating mode, CHP variable speed + PV		
Apartments	$P_{PV} = 17.9$ kW	$P_{PV} = 35.8$ kW	$P_{PV} = 53.7$ kW
100	7.06	7.87	8.56
50	11.70	12.67	13.32
30	13.94	14.84	15.24

the PV component within the integrated system, its output was increased twice and three times, with respect to the initial value.

Table 6 presents the results obtained in mixed operating mode, emphasizing the benefits derived from the integration with a PV array having a rated power of 17.9 kW. In mixed operating mode, the PES values are lower than those obtained in thermal priority mode, due to the heat waste occurring during the low thermal load periods. If we consider only the CHP unit, the variable speed control strategy increases the PES index by 20–25%, with an increment of only about 1 point in the case of 100 apartments up to about 2.5 points for 30 apartments. Regardless of the adopted CHP control strategy, the integrated system CHP + PV operates with better PES since it reduces the CHP unit operating load and time during the summer, and therefore the amount of wasted heat.

The data in Table 7 aim to characterize the influence of the PV array output on the integrated system performance. In addition to the case of PV array rated power of 17.9 kW, other two situations were considered, with powers that are 35.8 and 53.7 kW, respectively. The idea is that the overall number of apartments, supported by a single CHP unit, can be divided in two or three block of flats, each having a 17.9 kW PV array on its roof top. As anticipated by the previous results, the increase of the PV component improves the PES values, due to the decreasing of the CHP operation time during the summer period, and therefore to the decrease of the wasted heat.

Conclusions

The paper describes a simulation model built in MATLAB-Simulink, able to predict the performance of an integrated system composed of a CHP unit and a PV system. The model was calibrated with the experimental data obtained on a CHP unit with an electrical power output of 85 kW, based on a variable speed controlled ICE fueled with natural gas and a PV system with a rated power of 17.9 kW. The comparison between numerical and experimental data demonstrated a good accuracy of the simulation model.

The model was used to assess the possible benefits that may result from the CHP unit operation with variable speed strategy and from the integrated operation with the PV system. The results demonstrate that the thermal priority operating mode allows for the maximum PES values (about 21%), but with low time of full load operation, therefore with low level of electrical energy production. The mixed thermal/electrical priority operating mode could represent a solution to increase the electrical energy amount, even if the PES values are lower. In this case, the maximum calculated PES value was about 15%. Considering all analyzed cases, the ICE variable speed control strategy leads to a maximum increasing of the PES index by only two points, while in thermal priority operating mode, the same strategy has no effect on the PES index. Anyhow, the considered integrated CHP + PV plants can be classified as high efficiency ones, since the PES values are always higher than the limit specified by the European directive.

These results were obtained on the basis of some simplifying assumptions regarding the load profiles and the performances of both CHP and PV plants, and leaving aside any economic considerations, that could be possibly carried out as reported in Refs. [24] and [25]. However, also the more detailed energetic investigations required by real applications should confirm the main conclusions of the analysis. One of these was that, in order to obtain high values of the PES index, the CHP unit must be underutilized during summer to avoid wasting heat. Then, it might be interesting to carry out a thermo-economy comparison between the presented CHP–PV integrated system and a more conventional boiler–PV system.

Acknowledgment

The authors wish to thank Area Science Park of Trieste (Italy) for the granted support during the experimental phase.

Nomenclature

AFR = air fuel ratio
CCAB = control cabinet
CHP = combined heat and power
ICE = internal combustion engine
LHV = lower heating value
NTU = number of transfer units
PID = proportional-integral-derivative
PV = photovoltaic
STC = PV standard test condition (1000 W/m^2, 25 °C)

Greek Symbols

c = heat capacity (kJ/kg K)
$\dot{m}$ = mass flow rate (kg/s)
P = power (kW)
T = temperature (K)
x = fraction
γ = PV power temperature coefficient (°C^{-1})

Subscripts

c = engine coolant
el = electrical
ex = exhaust gas
f = fuel
hl = heat losses
m = mechanical
p = panel
ref = reference or reflection
sys = system
temp = temperature
th = thermal
w = water

References

[1] Commission of the European Communities, 2007, "An Energy Policy for Europe," Brussels, Belgium.
[2] Commission of the European Communities, 2008, "20 20 by 2020 Europe's Climate Change Opportunity," Brussels, Belgium.
[3] Directive 2004/8/EC of the European Parliament and of the Council, 2004, "On the Promotion of Cogeneration Based on a Useful Heat Demand in the Internal Energy Market and Amending Directive 92/42/EEC.
[4] Yun, K., Luck, R., Mago, P. J., and Smith, A., 2012, "Analytic Solutions for Optimal Power Generation Unit Operation in Combined Heating and Power Systems," ASME J. Energy Resour. Technol., **134**(1), p. 011301.
[5] Badami, M., Casetti, A., Campanile, P., and Anzioso, F., 2007, "Performance of an Innovative 120 kWe Natural Gas Cogeneration System," Energy, **32**(5), pp. 823–833.
[6] Badami, M., Mura, M., Campanile, P., and Anzioso, F., 2008, "Design and Performance Evaluation of an Innovative Small Scale Combined Cycle Cogeneration System," Energy, **33**(8), pp. 1264–1276.

[7] Caresana, F., Brandoni, C., Feliciotti, P., and Bartolini, C. M., 2011, "Energy and Economic Analysis of an ICE-Based Variable Speed-Operated Micro-Cogenerator," Appl. Energy, **88**(3), pp. 659–671.
[8] Sadeghi, S., and Ameri, M., 2014, "Exergy Analysis of Photovoltaic Panels-Coupled Solid Oxide Fuel Cell and Gas Turbine-Electrolyzer Hybrid System," ASME J. Energy Resour. Technol., **136**(3), p. 031201.
[9] Pearce, J. M., 2009, "Expanding Photovoltaic Penetration With Residential Distributed Generation From Hybrid Solar Photovoltaic and Combined Heat and Power Systems," Energy, **34**(11), pp. 1947–1954.
[10] Carmeli, M. S., Castelli-Dezza, F., Mauri, M., Marchegiani, G., and Rosati, D., 2012, "Control Strategies and Configurations of Hybrid Distributed Generation Systems," Renewable Energy, **41**(1), pp. 294–305.
[11] Rustica, G., Badami, M., and Portoraro, A., 2010, "Micro-cogenerazione nel settore residenziale con l'utilizzo di motori a combustione interna: Sviluppo di un modello matematico per la simulazione oraria e analisi di un caso reale," ENEA-RSE Report RdS/2010/x227.
[12] Duffie, J. A., William, A., and Beckman, W. A., 2006, *Solar Engineering of Thermal Processes*, 3rd ed., Wiley, Hoboken, NJ,
[13] Loutzenhiser, P. G., Manz, H., Felsmann, C., Strachan, P. A., Frank, T., and Maxwell, G. M., 2007, "Empirical Validation of Models to Compute Solar Irradiance on Inclined Surfaces for Building Energy Simulation," Sol. Energy, **81**(2), pp. 254–267.
[14] Micheli, D., Alessandrini, S., Radu, R., and Casula, I., 2014, "Analysis of the Outdoor Performance and Efficiency of Two Grid Connected Photovoltaic Systems in Northern Italy," Energy Convers. Manage., **80**, pp. 436–445.
[15] King, D. L., Boyson, W. E., and Kratochvil, J. A., 2004, "Photovoltaic Array Performance Model," Sandia National Laboratories, Report No. SAND2004-3535.
[16] SANYO Component Europe GmbH—Solar Division, 2008, "Sanyo HIT Photovoltaic Module," München, Germany.
[17] AVL List GmbH, 2011, "AVL BOOST Theory," Graz, Austria.
[18] AVL List GmbH, 2011, "AVL BOOST User's Guide," Graz, Austria.
[19] GM Powertrain, 2007, "Vortec 8100 Industrial Engine," Turin, Italy.
[20] Barbieri, E. S., Spina, P. R., and Venturini, M., 2012, "Analysis of Innovative Micro-CHP Systems to Meet Household Energy Demands," Appl. Energy, **97**, pp. 723–733.
[21] European Union, 2011, "Implementing the Energy Performance of Buildings Directive (EPBD)," Brussels, Belgium.
[22] Di Andrea, F., and Danese, A., 2004, "MICENE—Misure dei consumi di energia elettrica nel settore domestico," Dipartimento di Energetica—Politecnico di Milano, eERG, Milano, Italy.
[23] http://re.jrc.ec.europa.eu/pvgis/apps4/pvest.php
[24] Cullen, B., and McGovern, J., 2009, "The Quest for More Efficient Industrial Engines: A Review of Current Industrial Engine Development and Applications," ASME J. Energy Resour. Technol., **131**(2), p. 021601.
[25] Facci, A. L., Andreassi, L., Martini, F., and Ubertini, S., 2014, "Comparing Energy and Cost Optimization in Distributed Energy Systems Management," ASME J. Energy Resour. Technol., **136**(3), p. 032001.